
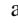
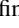


Effect of finite-rate catalysis on wall heat flux prediction in hypersonic flowF. Bonelli ^{1,*}, G. Pascazio ¹ and G. Colonna ²¹*Dipartimento di Meccanica Matematica e Management & Centro di Eccellenza in Meccanica Computazionale, Politecnico di Bari, via Re David 200, 70125 Bari, Italy*²*Istituto per la Scienza e Tecnologia dei Plasmi, Bari, Italy*

(Received 1 October 2020; accepted 19 February 2021; published 11 March 2021)

This work deals with the simulation of hypersonic flows past a copper sphere by using a finite-rate catalysis model coupled with either a state-to-state (StS) or a multitemperature thermochemical nonequilibrium approach. Without detailed state-specific data for copper catalytic recombination, molecules formed on the surface are described with three different statistics: one reproducing the incoming distribution, one considering a uniform distribution, and the third populating only the highest vibrational level. Following recent experimental and theoretical results, very high enthalpy and very low pressure conditions have been considered. The finite-rate partial catalysis model provides results that are closer to the experimental ones than those obtained by a fully catalytic approach. The multitemperature model shows better agreement with experiments, whereas among the StS catalytic approaches the outcomes have shown that the surface recombination on only the highest energy level gives more accurate results.

DOI: [10.1103/PhysRevFluids.6.033201](https://doi.org/10.1103/PhysRevFluids.6.033201)**I. INTRODUCTION**

A space capsule entering planetary atmosphere at hypersonic speed represents a well-known system in which strong chemical and thermal nonequilibrium conditions affect the shock wave structure and surface heat flux [1,2]. These are fundamental quantities required for the design of an efficient thermal protection system (TPS) of an atmosphere-entering vehicle [3,4]. Moreover, in recent years this problem has become of interest to estimate the danger due to uncontrolled bodies, such as debris [5] and meteoroids [6,7] entering the atmosphere.

Flow conditions downstream of the shock wave occurring in front of a body flying in a hypersonic regime at an altitude between 80 and 50 km [8] show high values of pressure (≈ 1 atm) and temperature ($> 10\,000$ K), conditions that are very difficult for any kind of material to withstand. To ensure that the heat shield is designed properly, an accurate prediction of the wall heat flux is mandatory. The effective heat flux reaching the vehicle surface has to be evaluated, taking into account radiative heating as well as conducting and convective contributions; radiative heating dominates in the case of superorbital reentry [9]. The heat flux is strongly dependent on the energy stored in the chemical processes and in internal degrees of freedom [10], on the one hand reducing the shock wave temperature, and on the other hand increasing the radiative heating. Ground test facilities (hypersonic wind tunnels) [11,12], which are devoted to reproducing in a laboratory the same conditions encountered during atmospheric entry, have very high operational costs. However, flows created in hypersonic wind tunnels, which are capable of reproducing pressure and temperature in the upper atmosphere, are in strong thermal and chemical nonequilibrium [13,14]. On the other hand, instrumented flight tests [15,16] have extremely high costs, considering that only

* Author to whom all correspondence should be addressed: francesco.bonelli@poliba.it

some quantities, such as the stand-off distance, the heat flux, and the body pressure profile, can be measured.

In this context, affordable numerical modeling is a primary factor in reducing the costs of the design procedure, and in investigating and predicting the conditions for an entry vehicle. Moreover, modeling can provide a deeper insight into the fundamental chemical-physical processes during vehicle reentry.

The most popular approach to accounting for thermochemical nonequilibrium is the multitemperature model [2], which considers the rotational and translational degrees of freedom in equilibrium at a common rotranslational temperature (T), whereas vibrational and electronic modes follow a Boltzmann internal distribution but at different temperatures (T_v and T_e). To account for the effects of thermal nonequilibrium on chemical reactions, Arrhenius rates are evaluated at an effective temperature calculated as the weighted geometrical mean of T and T_v . However, the assumption of having a Boltzmann distribution for vibrational and electronic excitation is not always verified, and it can lead to important inaccuracies in the evaluation of reaction rates [17]. To overcome this issue, the state-to-state (StS) approach [18,19] follows the evolution of each internal level, thus it can approximate their effective distribution. Such a capability incurs a larger computational cost than the multitemperature model does [20], and it requires large sets of rate coefficients resolved by the internal state in a wide temperature range [21–24] these data are available only for a limited number of processes. So far, very few multidimensional StS simulations have been performed [20–25]. Specifically, thanks to a message passing interface–compute unified device architecture (MPI-CUDA) implementation, the authors have been able to perform two-dimensional (2D) StS simulations on a GPU cluster [17–26] using a reasonable amount of computational time, comparable to that needed by a CPU parallel computation implementing a multitemperature model. A data parallelism approach with a single-program multiple data method (SPMD) and no task-based parallelism is employed. Multi-GPU computations are realized by using CUDA for running on GPUs, and MPI for data communications among GPUs (see Refs. [26–28]).

While in previous works [17–26] the authors focused their attention on the ability of the Park and StS models to predict the stand-off distance (a quantity often measured in experiments [29]), the present paper deals with an evaluation of wall heat flux. This is the most important quantity needed to properly design the TPS of a space capsule, and it is strictly related to the thermochemical model.

Recently, a test campaign commissioned by NASA was performed at the Italian Aerospace Research Centre (CIRA) using the SCIROCCO Plasma Wind Tunnel, an arc jet facility able to generate high enthalpy–low pressure hypersonic flows of large dimension [30]. Differently from past experiments (see Fig. 1 in Ref. [30]), these tests considered very high enthalpy and very low pressure in order to simulate superorbital entry.

A copper hemispherical probe was used to measure heat flux and pressure at the wall. Such measurements were used as a reference to assess the ability of numerical simulations to reproduce the experimental results. The CIRA group employed both a computational fluid dynamics (CFD) Navier-Stokes (NS) solver [31] and a direct simulation Monte Carlo (DSMC) code [32]. The results obtained by Cinquegrana *et al.* [30] solving the NS equations, with a fully catalytic wall, showed important deviations from the experiments (between 38% and 46.8%), overestimating the heat flux. To explain the mismatch, Cinquegrana *et al.* [30] argued that the continuum hypothesis was not satisfied, so they performed a further analysis with a DSMC approach (with a fully catalytic wall). They obtained better agreement, but the deviations were still significant (between 13.4% and 23.4%). It is important to notice that in such flow conditions, the Knudsen number is in the range of the continuous regime [33], making the use of the Navier-Stokes equation indeed effective. To bridge the gap, a further hypothesis was introduced by Cinquegrana *et al.* [30] assuming the copper surface in a partial catalytic condition and carrying out a parametric study by varying the recombination coefficient for both the NS and the DSMC computations. The results showed that, with a proper recombination coefficient, both NS and DSMC provide heat fluxes in agreement with the measured ones.

From such a study, it seems more reasonable that deviations from experimental findings are mainly due to the fully catalytic assumption, an unrealistic hypothesis for such flow conditions. As a consequence, a more accurate finite-rate catalysis model is required to enhance the prediction capability of the CFD solver.

To understand if the use of a more accurate thermochemical nonequilibrium model can play an important role in predicting the heat flux at the wall in such extreme conditions, the present work is intended to investigate the experimental tests in Ref. [30] by solving the NS equations with both the Park and the StS model, employing a more realistic finite-rate catalysis model [34].

It should be pointed out that in these conditions, ionization and electronic excitation could make a non-negligible contribution [35–37], and the shock wave can be affected by chemi-ionization processes as for hydrogen [38]. These aspects will be investigated in the future.

II. GOVERNING EQUATIONS AND NUMERICAL METHOD

High enthalpy flows are investigated by solving the Navier-Stokes equations for a reacting neutral air mixture (N_2 , O_2 , NO , N , and O) in an axial symmetric configuration. Single-component diffusive coefficients have been computed by using Gupta's [39] curve fits, whereas mixture properties have been evaluated with classical mixing rules [40–42]. Regarding thermochemical nonequilibrium, the Park model considers 5 species, 17 reactions, and 3 transport equations for vibrational energies of N_2 , O_2 , and NO . On the other hand, the StS approach considers 68 vibrational levels for N_2 , 47 for O_2 , and only the ground state for NO .

Equations are solved by using a finite-volume solver with a multiblock structured body-fitted mesh. Convective terms of the frozen Navier-Stokes equations are solved by employing Steger-Warming [43] flux vector splitting with a second-order MUSCL reconstruction, whereas the Gauss divergence theorem with a linear interpolation is employed to compute the derivatives of viscous terms. An operator splitting approach is employed to separate fluid dynamics from stiff chemical kinetics. Time integration of the frozen equations is performed by employing an explicit Runge-Kutta scheme, whereas stiff chemical kinetics is handled by using an implicit Gauss-Seidel algorithm.

More details on equations, models, and the high-performance computing approach can be found in Refs. [17,26–28,44].

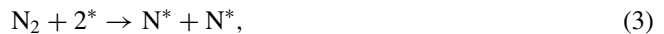
A. Heterogeneous catalysis model

To account for a partially catalytic wall, a finite-rate model has been employed. Inspired by the work of Armenise *et al.* [34], the finite-rate catalytic model considers the following heterogeneous processes:

- (i) Atom chemisorption (ch) on an active site $*$ to form an adatom A^* ,



- (ii) molecule chemisorption (chdm),



- (iii) the Eley-Rideal recombination mechanisms (ER),

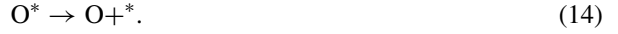




(iv) the Langmuir-Hinshelwood recombination mechanisms (LH),



(v) the thermal desorption mechanism (td),



The law of mass action provides the rate equations for $[\text{N}^*]$ and $[\text{O}^*]$,

$$\begin{aligned} \frac{d[\text{N}^*]}{dt} = & [\text{N}][\text{S}]k_{\text{ch}}^{\text{N}} + 2[\text{N}_2][\text{S}]^2k_{\text{chdm}}^{\text{N}_2} + [\text{NO}][\text{S}]^2k_{\text{chdm}}^{\text{NO}} \\ & - [\text{N}][\text{N}^*]k_{\text{ER}}^{\text{NN}} - [\text{O}][\text{N}^*]k_{\text{ER}}^{\text{ON}} - 2[\text{N}^*][\text{N}^*]k_{\text{LH}}^{\text{NN}} \\ & - [\text{N}^*][\text{O}^*]k_{\text{LH}}^{\text{NO}} - [\text{N}^*]k_{\text{td}}^{\text{N}}, \end{aligned} \quad (15)$$

$$\begin{aligned} \frac{d[\text{O}^*]}{dt} = & [\text{O}][\text{S}]k_{\text{ch}}^{\text{O}} + 2[\text{O}_2][\text{S}]^2k_{\text{chdm}}^{\text{O}_2} + [\text{NO}][\text{S}]^2k_{\text{chdm}}^{\text{NO}} \\ & - [\text{O}][\text{O}^*]k_{\text{ER}}^{\text{OO}} - [\text{N}][\text{O}^*]k_{\text{ER}}^{\text{NO}} - 2[\text{O}^*][\text{O}^*]k_{\text{LH}}^{\text{OO}} \\ & - [\text{N}^*][\text{O}^*]k_{\text{LH}}^{\text{NO}} - [\text{O}^*]k_{\text{td}}^{\text{O}}, \end{aligned} \quad (16)$$

where $([\text{S}] = [\text{S}_0] - [\text{N}^*] - [\text{O}^*])$ is the number of unoccupied sites per unit area, and $[\text{S}_0]$ is the number of active sites per unit area, where reaction rate coefficients are expressed in the Arrhenius form as given in Refs. [34,45]. For an efficient implementation of finite-rate catalytic wall boundary conditions, atomic recombination coefficients of species A and B have been employed:

$$\gamma_{AB} = \frac{\text{Flux of atoms recombining at the surface}}{\text{Flux of atoms impinging on the surface}}. \quad (17)$$

In the present work, four recombination coefficients have been considered, i.e., γ_{NN} due to the heterogeneous processes (3), (6), and (10), γ_{OO} due to (4), (7), and (11), and γ_{NO} and γ_{ON} due to (5), (8), (9), and (12), whose expressions are therefore [34]

$$\gamma_{\text{NN}} = \frac{2(-[\text{N}_2][\text{S}]^2k_{\text{chdm}}^{\text{N}_2} + [\text{N}][\text{N}^*]k_{\text{ER}}^{\text{NN}} + [\text{N}^*]^2k_{\text{LH}}^{\text{NN}})}{Z_{\text{N}}}, \quad (18)$$

$$\gamma_{\text{OO}} = \frac{2(-[\text{O}_2][\text{S}]^2k_{\text{chdm}}^{\text{O}_2} + [\text{O}][\text{O}^*]k_{\text{ER}}^{\text{OO}} + [\text{O}^*]^2k_{\text{LH}}^{\text{OO}})}{Z_{\text{O}}}, \quad (19)$$

$$\gamma_{\text{NO}} = \frac{(-[\text{NO}][\text{S}]^2k_{\text{chdm}}^{\text{NO}} + [\text{N}][\text{O}^*]k_{\text{ER}}^{\text{NO}} + [\text{O}][\text{N}^*]k_{\text{ER}}^{\text{ON}} + [\text{N}^*][\text{O}^*]k_{\text{LH}}^{\text{NO}})}{Z_{\text{N}}}, \quad (20)$$

$$\gamma_{\text{ON}} = \frac{(-[\text{NO}][\text{S}]^2k_{\text{chdm}}^{\text{NO}} + [\text{N}][\text{O}^*]k_{\text{ER}}^{\text{NO}} + [\text{O}][\text{N}^*]k_{\text{ER}}^{\text{ON}} + [\text{N}^*][\text{O}^*]k_{\text{LH}}^{\text{NO}})}{Z_{\text{O}}}, \quad (21)$$

where $Z_A = [A]\sqrt{kT/(2\pi m_A)}$, with $A = \text{N}, \text{O}$, k is the Boltzmann constant, and m is the atomic mass. In this work, a copper surface has been considered for which N_2 and NO cannot be chemisorbed [34], therefore Eqs. (15), (16), (18), (20), and (21) become

$$\begin{aligned} \frac{d[\text{N}^*]}{dt} = & [\text{N}][\text{S}]k_{\text{ch}}^{\text{N}} - [\text{N}][\text{N}^*]k_{\text{ER}}^{\text{NN}} - [\text{O}][\text{N}^*]k_{\text{ER}}^{\text{ON}} \\ & - 2[\text{N}^*][\text{N}^*]k_{\text{LH}}^{\text{NN}} - [\text{N}^*][\text{O}^*]k_{\text{LH}}^{\text{NO}} - [\text{N}^*]k_{\text{id}}^{\text{N}}, \end{aligned} \quad (22)$$

$$\begin{aligned} \frac{d[\text{O}^*]}{dt} = & [\text{O}][\text{S}]k_{\text{ch}}^{\text{O}} + 2[\text{O}_2][\text{S}]^2k_{\text{chdm}}^{\text{O}_2} - [\text{O}][\text{O}^*]k_{\text{ER}}^{\text{OO}} \\ & - [\text{N}][\text{O}^*]k_{\text{ER}}^{\text{NO}} - 2[\text{O}^*][\text{O}^*]k_{\text{LH}}^{\text{OO}} - [\text{N}^*][\text{O}^*]k_{\text{LH}}^{\text{NO}} \\ & - [\text{O}^*]k_{\text{id}}^{\text{O}}, \end{aligned} \quad (23)$$

$$\gamma_{\text{NN}} = \frac{2([\text{N}][\text{N}^*]k_{\text{ER}}^{\text{NN}} + [\text{N}^*]^2k_{\text{LH}}^{\text{NN}})}{Z_{\text{N}}}, \quad (24)$$

$$\gamma_{\text{NO}} = \frac{([\text{N}][\text{O}^*]k_{\text{ER}}^{\text{NO}} + [\text{O}][\text{N}^*]k_{\text{ER}}^{\text{ON}} + [\text{N}^*][\text{O}^*]k_{\text{LH}}^{\text{NO}})}{Z_{\text{N}}}, \quad (25)$$

$$\gamma_{\text{ON}} = \frac{([\text{N}][\text{O}^*]k_{\text{ER}}^{\text{NO}} + [\text{O}][\text{N}^*]k_{\text{ER}}^{\text{ON}} + [\text{N}^*][\text{O}^*]k_{\text{LH}}^{\text{NO}})}{Z_{\text{O}}}. \quad (26)$$

In the case of the StS model, three approaches have been considered to determine the distribution of the desorbed molecules. In the first approach (named StS-1), $\gamma_{\text{NN}}(l)$, where l is the l th vibrational level, is computed as $\gamma_{\text{NN}}(l) = \gamma_{\text{NN}} \frac{\rho_{\text{N}_2, l}}{\rho_{\text{N}_2}}$, whereas

$$\gamma_{\text{OO}}(l) = \frac{2(-[\text{O}_{2, l}][\text{S}]^2k_{\text{chdm}}^{\text{O}_2} + ([\text{O}][\text{O}^*]k_{\text{ER}}^{\text{OO}} + [\text{O}^*]^2k_{\text{LH}}^{\text{OO}}) \frac{\rho_{\text{O}_2, l}}{\rho_{\text{O}_2}})}{Z_{\text{O}}}. \quad (27)$$

In the second approach (named StS-2), a uniform vibrational distribution has been considered, i.e., $\gamma_{\text{NN}}(l) = \gamma_{\text{NN}}/68$ and $\gamma_{\text{OO}}(l) = \gamma_{\text{OO}}/47$. In the third approach (named StS-3), the global recombination coefficients have been assumed to populate only the highest vibrational level.

Therefore, the recombination coefficients are used to compute the wall normal species derivatives at the wall [34], which in the most general case read

$$\left. \frac{\partial Y_{\text{N}}}{\partial n} \right|_w = \left(\sum_l \gamma_{\text{NN}}(l) + \gamma_{\text{NO}} \right) \frac{Y_{\text{N}}}{D_{\text{N}}} \sqrt{\frac{kT}{2\pi m_{\text{N}}}}, \quad (28)$$

$$\left. \frac{\partial Y_{\text{N}_2}(l)}{\partial n} \right|_w = -\frac{\gamma_{\text{NN}}(l)}{D_{\text{N}}} \sqrt{\frac{kT}{2\pi m_{\text{N}}}} Y_{\text{N}}, \quad (29)$$

$$\left. \frac{\partial Y_{\text{O}}}{\partial n} \right|_w = \left(\sum_l \gamma_{\text{OO}}(l) + \gamma_{\text{ON}} \right) \frac{Y_{\text{O}}}{D_{\text{O}}} \sqrt{\frac{kT}{2\pi m_{\text{O}}}}, \quad (30)$$

$$\left. \frac{\partial Y_{\text{O}_2}(l)}{\partial n} \right|_w = -\frac{\gamma_{\text{OO}}(l)}{D_{\text{O}}} \sqrt{\frac{kT}{2\pi m_{\text{O}}}} Y_{\text{O}}, \quad (31)$$

$$\left. \frac{\partial Y_{\text{NO}}(l)}{\partial n} \right|_w = -\frac{\gamma_{\text{ON}}}{D_{\text{O}}} \sqrt{\frac{kT}{2\pi m_{\text{O}}}} Y_{\text{O}} - \frac{\gamma_{\text{NO}}}{D_{\text{N}}} \sqrt{\frac{kT}{2\pi m_{\text{N}}}} Y_{\text{N}}, \quad (32)$$

where Y and D are the mass fraction and the mixture component diffusion coefficient, respectively.

TABLE I. Experimental test conditions [30].

Test ID	H_0 (MJ/kg)	P_0 (bar)	p_{exit} (mbar)	q_{probe} (kW/m ²)	p_{probe} (mbar)
396	23.8	2.5	0.24	1543	17.9

III. THE COMPUTATIONAL SETUP

The computational setup rebuilds the experimental one carried out at CIRA [30] in the SCIROCCO Plasma Wind Tunnel. The test case considered in this work is the one identified with the ID number 396 in the work of Cinquegrana *et al.* [30] (see Table I). The stagnation enthalpy and the stagnation pressure are, respectively, $H_0 = 23.8$ MJ/kg and $P_0 = 2.5$ bar. The conical nozzle has a divergent section 3.1 m long and an exit diameter equal to 1.1 m. At 37.5 cm from the nozzle exit section, a water-cooled hemispherical copper probe, with a diameter (D) of 10 cm, is located on the jet centerline. The probe wall temperature is fixed at $T_w = 300$ K. Unlike the multitemperature Park approach, StS models do not impose vibrational temperatures at the wall since they come out from vibrational levels of recombining molecules.

The hypersonic nozzle flow and the hypersonic flow past the probe have been simulated separately. Differently from the probe, the nozzle has been simulated by considering a noncatalytic wall at $T_w = 300$ K. To characterize the flow conditions at the probe location, a longer divergent section (3.5 m) has been considered. Such conditions have been employed as inflow for the simulation of the probe (see Table II), to take into account the strong thermal and chemical nonequilibrium at the nozzle exit [13].

By considering freestream conditions provided by the Park model, the Knudsen number has been evaluated under the assumption of a Maxwellian-Boltzmann distribution of molecules for which

$$\text{Kn} = \frac{\lambda}{D} = \frac{M}{\text{Re}_D} \sqrt{\frac{\pi c_p}{2c_v}} = 9.7 \times 10^{-3}, \quad (33)$$

where λ is the mean free path, D is the probe diameter, M is the freestream Mach number, Re_D is the Reynolds number, and c_p and c_v are the specific heat at constant pressure and constant volume, respectively. The Knudsen number is equal to 9.7×10^{-3} , smaller enough than 0.03, which is the upper limit for the continuous regime [33], therefore the use of the Navier-Stokes equations is effective.

The stagnation flow conditions for the nozzle simulation have been evaluated by a 0D air equilibrium computation with fixed H_0 and P_0 . Taking advantage of the axial symmetric conditions, a half nozzle has been simulated by using a computational grid that includes 280×72 fluid cells,

TABLE II. Freestream conditions for probe calculations.

Parameter	Park	StS
H_0 (MJ/kg)	23.8	23.8
P_∞ (Pa)	18.34	15.85
u_∞ (m/s)	5055	4906
T_∞ (K)	560.7	449.9
ρ_∞ (kg/m ³)	8.092×10^{-5}	8.504×10^{-5}
$Y_{\text{N}_2, \infty}$	5.806×10^{-1}	5.468×10^{-1}
$Y_{\text{O}_2, \infty}$	4.263×10^{-8}	3.871×10^{-7}
$Y_{\text{NO}, \infty}$	1.489×10^{-5}	1.302×10^{-11}
$Y_{\text{N}, \infty}$	1.895×10^{-1}	2.204×10^{-1}
$Y_{\text{O}, \infty}$	2.298×10^{-1}	2.327×10^{-1}

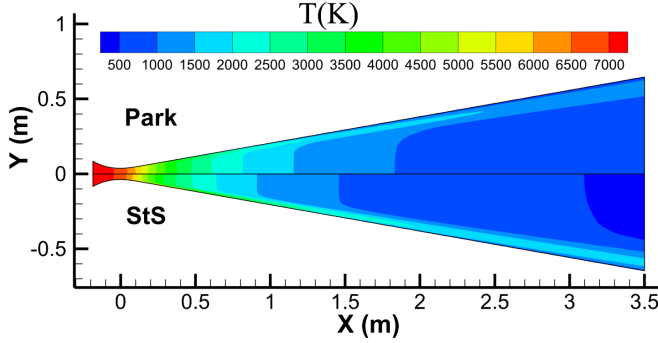


FIG. 1. Nozzle flow: gas rototranslational temperature contour plot obtained by using both the Park (top) and the StS (bottom) models.

whereas a quarter of a sphere is simulated by using a computational grid, which includes 228×393 fluid cells with a finer resolution both near the wall and the curved shock region.

IV. RESULTS

Figure 1 shows the gas rototranslational temperature contour plot inside the nozzle obtained by using both the Park and the StS model: StS provides a lower temperature in the divergent part of the nozzle. As shown in Fig. 2, along the nozzle centerline Park and StS models provide qualitatively similar temperature profiles for rototranslational and nitrogen molecule vibrational mode but a quite different vibrational temperature of oxygen molecules ($T_v^{O_2}$). Both models show a much higher vibrational temperature of nitrogen molecules ($T_v^{N_2}$) with respect to the gas temperature. On the other hand, the Park model provides an extremely low vibrational temperature of oxygen molecules in the divergent section (about 9 K at $x = 3.5$ m), whereas a $T_v^{O_2}$ higher than the gas temperature but lower than $T_v^{N_2}$ is given by the StS model. The StS results can lead to the wrong conclusion

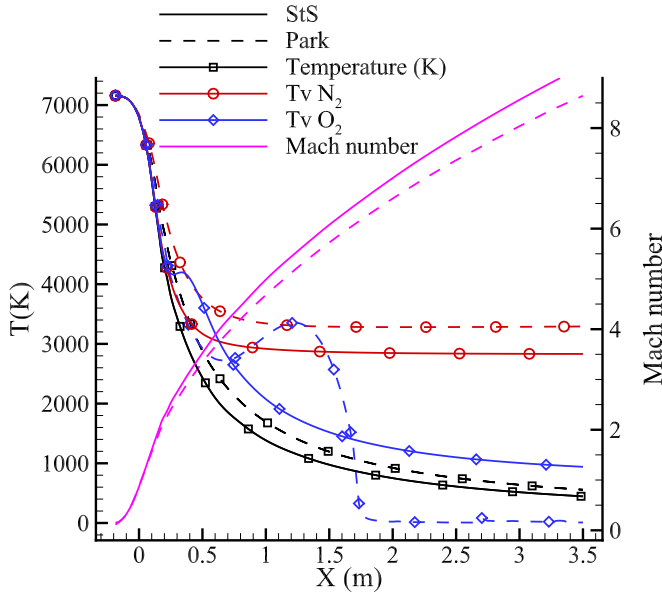


FIG. 2. Nozzle flow: rototranslational temperature, vibrational temperature, and Mach number profiles along the nozzle axis.

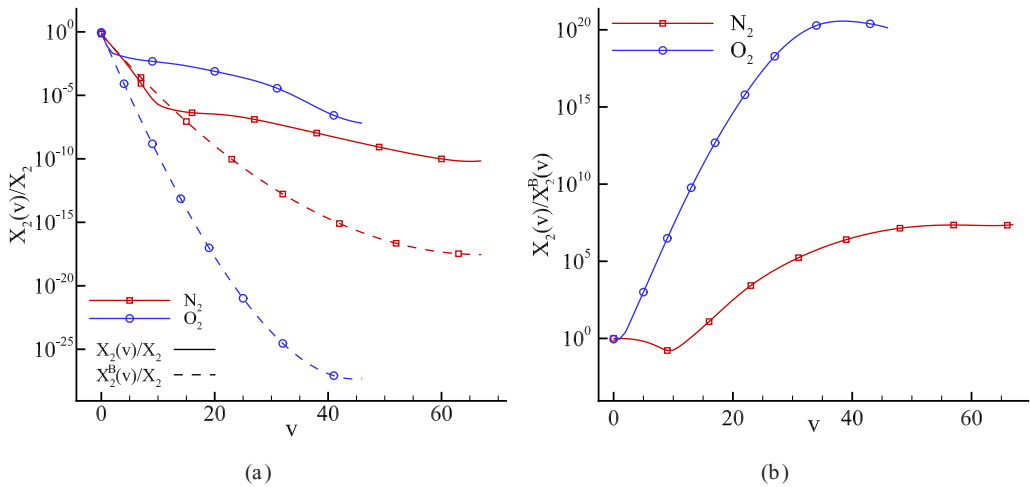


FIG. 3. Nozzle flow distributions at $x = 3.5$ m along the axis: (a) N_2 and O_2 populations; (b) actual to Boltzmann ratio.

that thermal nonequilibrium is larger for nitrogen molecules. However, looking at the distributions shown in Fig. 3(a), it is evident that at $x = 3.5$ m both oxygen and nitrogen molecules show a significant overpopulation of high-energy levels that is even larger for oxygen, as highlighted by the ratio between the computed distribution and the Boltzmann one [see Fig. 3(b)]. This behavior is a consequence of the larger oxygen atom concentration that, on the one hand, speeds up the thermalization of the low vibrational levels of O_2 through νT (vibration-translation) processes, and on the other hand, increases the recombination that is responsible for the overpopulation of the distribution tail. The different behaviors of the two models could be attributed to the way the recombination energy is assigned to the vibrational degree of freedom, explaining also the bump in its vibrational temperature. Figures 4(a) and 4(b) show that species mass fractions become frozen in the divergent section with some exceptions: the Park model shows a further dissociation of

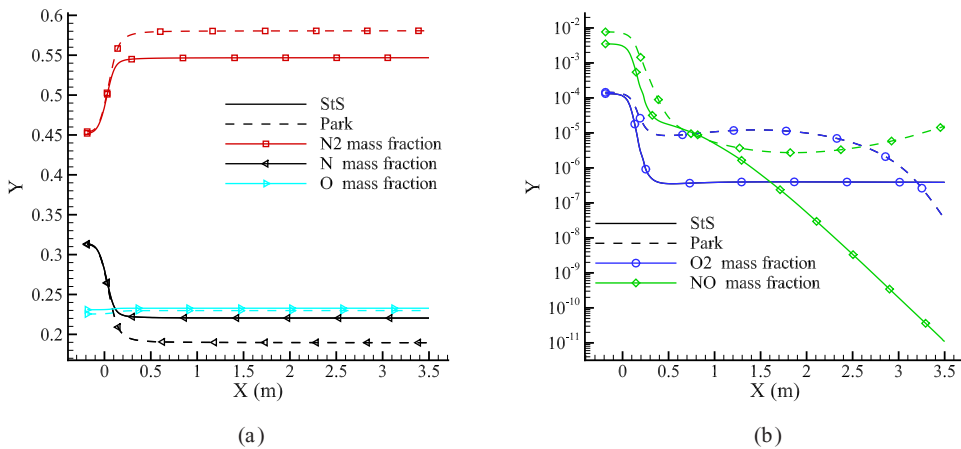


FIG. 4. Nozzle flow: species mass fractions along the axis: (a) linear scale, (b) log scale.

TABLE III. Nozzle axial exit pressure (at $x = 3.1$ m): experiments, Park and StS with noncatalytic wall and Ref. [30]. Probe stagnation pressure and heat flux at stagnation point obtained as follows: experimentally, by the partially catalytic model: Park, StS-1, StS-2, and StS-3 (StS models differ only for catalytic condition on the probe wall); by a fully catalytic (FC) approach at the sphere wall: Park, by Cinquegrana *et al.* [30]: Park, DSMC.

	Expt.	Park (err. %)	StS/ StS-1 (err. %)	StS-2 (err. %)	StS-3 (err. %)	Park FC (err. %)	Ref. [30] Park FC (err. %)	Ref. [30] DSMC FC (err. %)
p_{exit} (mbar)	0.24	0.2483 (3.46%)	0.2153 (10.3%)				0.24 (0%)	
p_{probe} (mbar)	17.9	18.49 (3.30%)	18.13 (1.28%)	18.16 (1.45%)	18.20 (1.66%)	19.03 (6.31%)	18.9 (5.59%)	19.0 (6.14%)
q_{probe} (kW/m ²)	1543	1708 (10.8%)	1873 (21.38%)	1816 (17.69%)	1774 (14.97%)	2160 (39.99%)	2211 (43.29%)	1750 (13.41%)

oxygen molecules upon approaching the exit, whereas the StS model predicts dissociation of NO molecules. The oxygen dissociation observed approaching the exit predicted by the Park model causes a large reduction of $T_v^{\text{O}_2}$ due to the chemical contribution to the vibrational temperature source term. The lower vibrational temperature of oxygen with respect to nitrogen as well as the larger nonequilibrium of the distribution tails are a consequence of its larger dissociation degree, which increases the speed of low-energy state relaxation through νT by atoms and at the same time increases recombination in high-energy levels.

Table III shows the values of the nozzle axial exit pressure (at $x = 3.1$ m) of the probe stagnation pressure and of the heat flux at the stagnation point obtained experimentally and by the computational approaches. With regard to the sphere, a fully catalytic (FC) computation was also performed by using the multitemperature model, thus the results of Cinquegrana *et al.* [30] are also given for comparison. The Park model predicts a pressure value at the nozzle exit that is very close to the experimental one, whereas a smaller value is provided by the StS approach. A better agreement of the partial catalytic Park model with experimental findings has also been found in terms of heat flux. Among the three StS approaches, the StS-3, which assumes that recombination at the wall populates only the highest energy level, provides better results in terms of heat flux at the stagnation point. Concerning the value of stagnation pressure, all models provide quite good results. It is also evident that the fully catalytic approach strongly overestimates the heat flux at the sphere wall, thus showing that in this case involving a very low wall temperature, the FC assumption is not realistic, as confirmed by the results of Cinquegrana *et al.* [30] given in Table III.

Table IV shows the heat flux evaluated at three different azimuthal angles (0° , 30° , 60°). Again, the partial catalytic Park model shows a better agreement with experiments. However, all models present larger deviations at increasing angles.

TABLE IV. Heat flux (kW/m²) on the sphere wall at different azimuthal angles.

Deg	Expt.	Park (err. %)	StS-1 (err. %)	StS-2 (err. %)	StS-3 (err. %)	Park FC (err. %)
0	1543	1708 (10.69%)	1873 (21.38%)	1816 (17.69%)	1774 (14.97%)	2160 (39.99%)
30	1139	1319 (15.80%)	1448 (27.13%)	1401 (23.00%)	1383 (21.42%)	1689 (48.29%)
60	486	591 (21.60%)	666 (37.04%)	651 (33.95%)	647 (33.13%)	812 (67.08%)

TABLE V. Decomposition of the total heat flux (kW/m²) and relative contribution at the stagnation point in rototranslational, diffusive, and vibrational contributions.

	Park	StS-1	StS-2	StS-3	Park FC
rototranslational	1082	1213.3	1516.0	1763.8	1146.6
(% contribution)	(63.34%)	(64.78%)	(83.48%)	(99.41%)	(53.07%)
diffusive	606.10	660.17	300.0	10.38	1000.5
(% contribution)	(35.48%)	(35.25%)	(16.52%)	(0.59%)	(46.31%)
vibrational	20.18				13.3
(% contribution)	(1.18%)				(0.62%)

Finally, Table V provides values of different contributions to the total heat flux. Indeed, the total heat flux can be decomposed into a rototranslational contribution given by the Fourier law,

$$q_{tw} = \lambda_t \nabla T|_w \cdot \mathbf{n}_w, \quad (34)$$

a vibrational contribution (only for the Park model),

$$q_{v_w} = \sum_m \lambda_{\text{vib},m} \nabla T_{v,m}|_w \cdot \mathbf{n}_w, \quad (35)$$

and a diffusive contribution due to catalytic recombination at the wall,

$$q_{d_w} = \sum_s \sum_l h_{s,l} \rho D_s \nabla Y_{s,l}|_w \cdot \mathbf{n}_w, \quad (36)$$

where T and $T_{v,m}$ are the rototranslational and the vibrational temperature, respectively; ρ is the gas density; λ_t and $\lambda_{\text{vib},m}$ are the rototranslational and the vibrational conductivity, respectively; $h_{s,l}$ is the specific enthalpy including translational-rotational, vibrational, and formation contributions; D_s is the mixture component diffusion coefficient; Y is the mass fraction; and m , s , and l are the generic molecule, the generic component, and the generic vibrational level, respectively. Again, it is evident that the FC assumption is not valid because an important contribution to the overestimation of the total heat flux is given by the diffusive flux with about 46% of the total. With regard to the partial catalytic approach, the rototranslational Fourier contribution is the most important for all models considered. However, for both the Park and the StS-1 approaches, the diffusive contribution is very important, being equal to about 35%, whereas it is lower, about 17%, in the case of the StS-2 approach, and negligible (less than 1%) when the StS-3 model is employed. Finally, the vibrational contribution, provided only by the Park model, is negligible.

Among state-to-state models, StS-3 gives better results because in populating the highest vibrational level, it reduces the diffusive contribution of the heat flux at the wall (see Table V), which seems to be the one that is overestimated by all the models. However, StS coefficient uncertainties have an impact on gas composition that determines the amount of atoms that can potentially recombine at the wall, thus having an important effect on chemical heat flux.

Figures 5(a) and 5(b) show that the pressure contour plots obtained by using the different approaches considered in this work are almost the same. Stagnation line temperature profiles provided in Figs. 6(a) and 6(b) show a smeared shock wave and a postshock rototranslational gas temperature of about 10 000 K with a higher value provided by the Park model. As in the case of the nozzle flow, significant differences emerge between the vibrational temperature obtained by using the Park and the StS approach. The Park model provides a nitrogen vibrational temperature that increases in the thermal boundary layer up to about 20 000 K before being imposed to 300 K at the wall. Such behavior is due to nitrogen recombination, which is taken into account in the chemical part of the vibrational temperature source term. With regard to the StS approaches [see Fig. 6(b)], the oxygen vibrational temperature shows a smaller relaxation time than the nitrogen

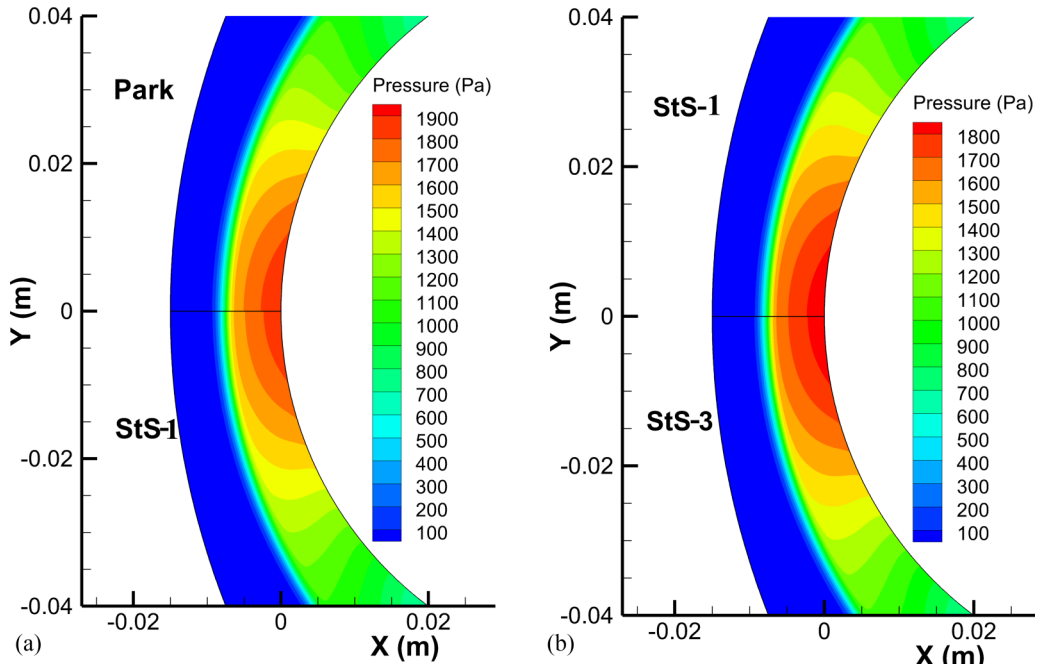


FIG. 5. Flow past a sphere: pressure contour plot: (a) Park and StS-1; (b) StS-1 and StS-3.

one by almost following the gas rototranslational temperature across the shock wave. However, downstream of the shock, $T_v^{O_2}$ decreases more quickly than the gas temperature in the case of the StS-1 approach, whereas it is closer to the translational temperature when the StS-3 approach is employed. An intermediate behavior is provided by the StS-2 model. On the other hand, the nitrogen vibrational temperature remains almost frozen in the shock layer for all StS models. It is also very

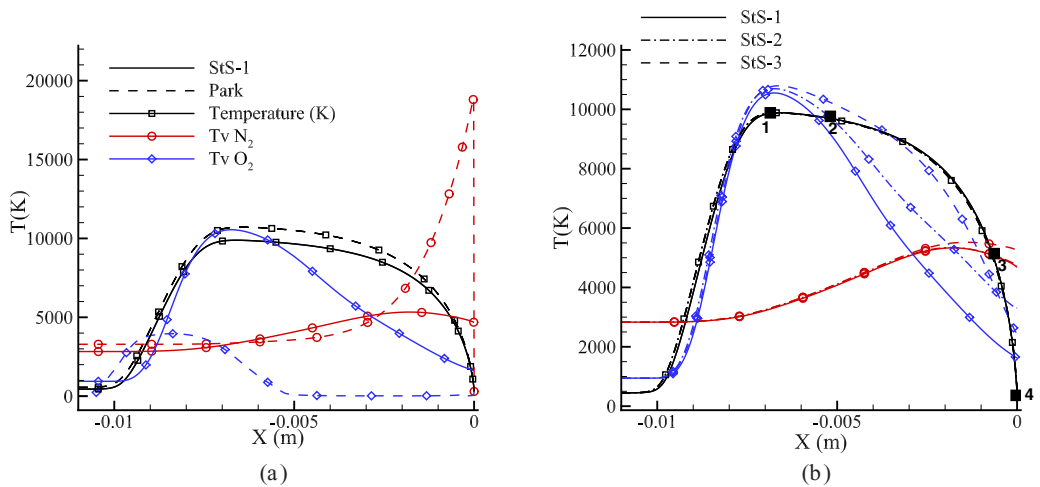


FIG. 6. Flow past a sphere: stagnation line temperature profiles. Points 1, 2, 3, and 4 show the location along the stagnation line where vibrational distributions have been evaluated (see Figs. 9 and 10).

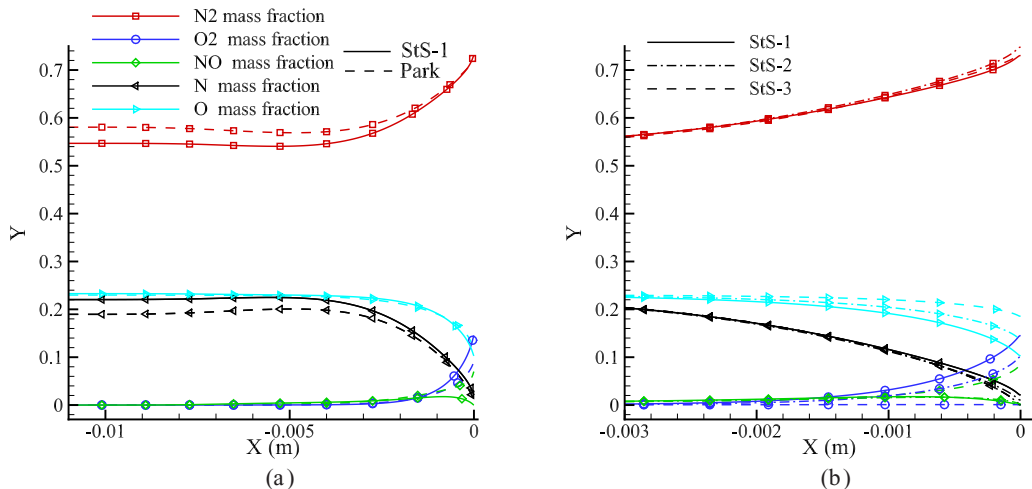


FIG. 7. Flow past a sphere: stagnation line mass fractions: (a) comparison with Park; (b) comparison among StS models.

important to note that when the StS models are employed, vibrational temperature is not fixed at the wall, and a strong nonequilibrium is observed.

Figures 7(a) and 7(b) show the mass fraction profiles along the stagnation line obtained by using the different models. Figure 7(a) shows that the StS-1 model predicts a larger recombination of N₂ and O₂, whereas it predicts a smaller recombination of NO with respect to the Park model. On the other hand, when the StS-3 model is employed, O₂ is not formed at the wall [see Fig. 7(b)], but there is a larger NO recombination at the wall with respect to the one provided by the StS-1 approach. Intermediate outcomes are provided by the StS-2 model.

Recombination coefficients along the wall as a function of the azimuthal angle are shown in Fig. 8. The StS-1 model provides the larger γ_{NN} and γ_{NO} , whereas the StS-3 model provides the smaller ones. The opposite behavior is shown for γ_{OO} and γ_{ON} . The Park model provides a γ_{NN} very close to the optimum value of 0.03 suggested by Cinquegrana *et al.* [30].

Stagnation line populations of N₂ and O₂, obtained by using the StS-1 approach, are given in Figs. 9(a) and 9(b); the actual to Boltzmann ratio is also shown in the inset. Populations have been evaluated along the stagnation streamline and downstream of the shock wave at probes 1, 2, and 3, whose locations are given in Fig. 6(b). N₂ shows a strong deviation from the Boltzmann distribution just downstream of the shock wave, whereas O₂ follows a Boltzmann distribution downstream of the shock wave, but it is far from Boltzmann in the thermal boundary layer. It should be noted that the azimuthal angular dependence of the distributions along the surface is negligible in the range 0°–60°, where thermal flux sensors are positioned.

To put in evidence the effects of the wall recombination model on the population of vibrational levels, Fig. 10 depicts N₂ and O₂ vibrational distributions computed at three points along the stagnation line [see Fig. 6(b)]: at the wall ($x_4 = 0$), inside the thermal boundary layer ($x_3 = -0.069$ cm), and at its limit, fixed at $x_2 = -0.526$, where the gradient of the species concentration becomes negligible. In this last point, the effects of the wall recombination model are practically negligible, while large differences among the three models are observed inside the boundary layer. The contribution of atomic nitrogen recombination is small because its mass fraction close to the wall is below 2% (see Fig. 7). This behavior is reflected in the distribution, and the effects of the wall recombination are more pronounced in O₂ than in N₂ vibrational populations. Indeed, only the distributions at the wall for the StS-2 model show overpopulated tails for $v > 20$, while differences between StS-1 and StS-3 are small, with a slight overpopulation of high-energy levels ($v > 35$) at

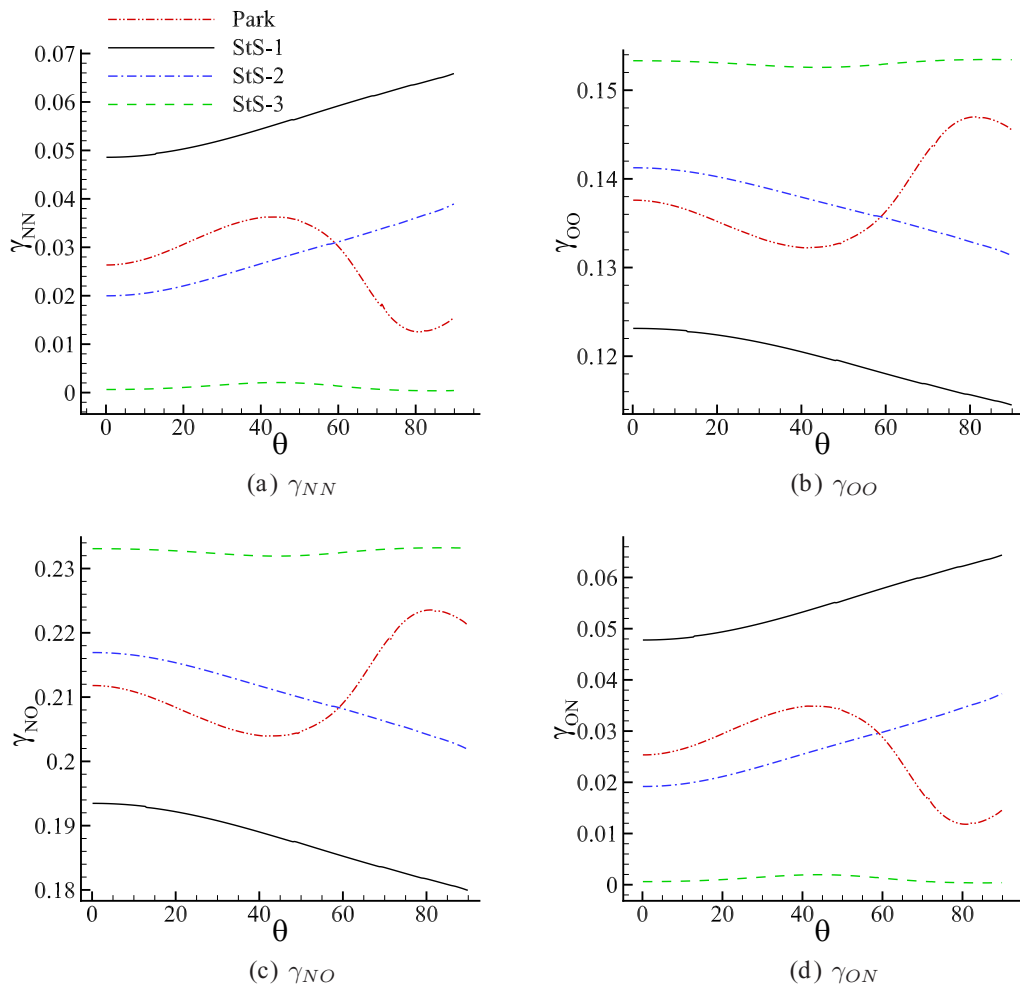


FIG. 8. Flow past a sphere: wall recombination coefficients as a function of the azimuthal angle θ [deg].

the wall. This result leads to the conclusion that the thermalization in the gas phase due to VV (vibration-vibration) and νT dominates in the boundary layer.

The O_2 vibrational distributions are strongly affected by the wall recombination model, and the shape of the distribution tail is a result of the balance between recombination and νTa (vibration-translation with atom) depletion. In the case of StS-1, no contribution comes from wall recombination because the exit distribution is the same as the impinging one. Because the StS-2 model distributes the molecules formed on the surface homogeneously, the distribution tail is almost flat at the wall, while at $x3$ it is depleted by νT . On the other hand, the StS-3 model populates the last vibrational level, and these molecules are redistributed to lower ν by νT . As a result, more energy is trapped in the vibrational levels, with the consequence of less energy transferred to the wall and a higher oxygen atom fraction, due to the rapid dissociation from highly excited states, and, therefore, reducing also the diffusive heat flux.

At present, a final statement about the most physically believable or consistent approach cannot be given. The first recombination approach (StS-1) is physically inconsistent, because the output distribution depends on the input one. StS-2 takes into account the calculated values for atomic nitrogen recombination on silica [46] and atomic oxygen on quartz [47], whereas StS-3 is constructed by analogy with gas phase recombination.

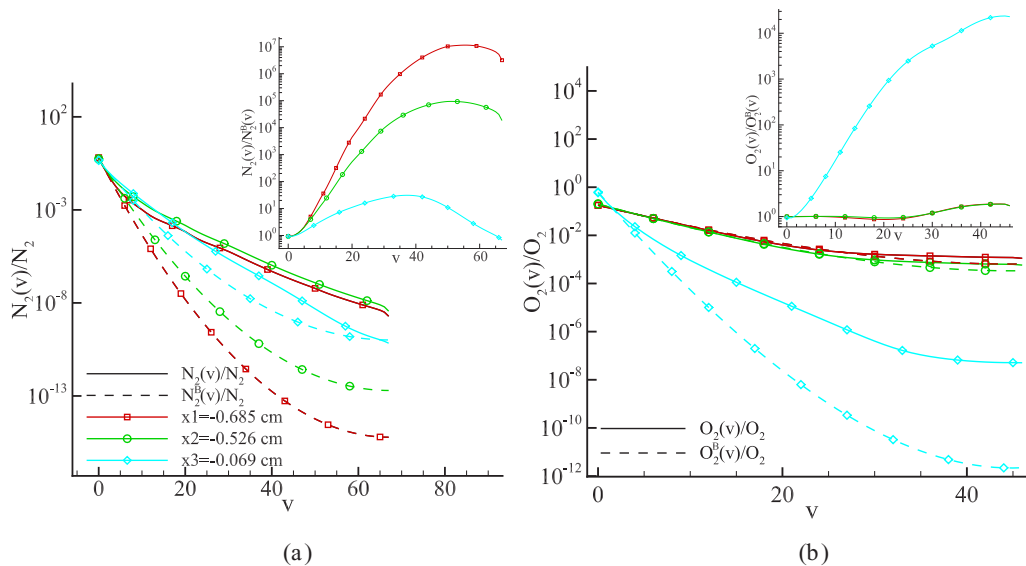


FIG. 9. Flow past a sphere: StS-1 approach: stagnation line populations with actual to Boltzmann ratio in the inset: (a) N_2 and (b) O_2 . Populations have been evaluated along the stagnation streamline and downstream of the shock wave at probes 1, 2, and 3, whose locations are given in Fig. 6(b).

V. CONCLUSIONS

In the present work, a 2D axial-symmetric solver of the Navier-Stokes equation has been employed in order to analyze numerical experiments performed in the SCIROCCO Plasma Wind Tunnel at CIRA. For such experiments, characterized by very high enthalpies and low pressure, Cinquegrana *et al.* [30] have shown that the Navier-Stokes equation with a fully catalytic assumption at the wall strongly overestimates the total heat flux. They argue that this is due to both a partial

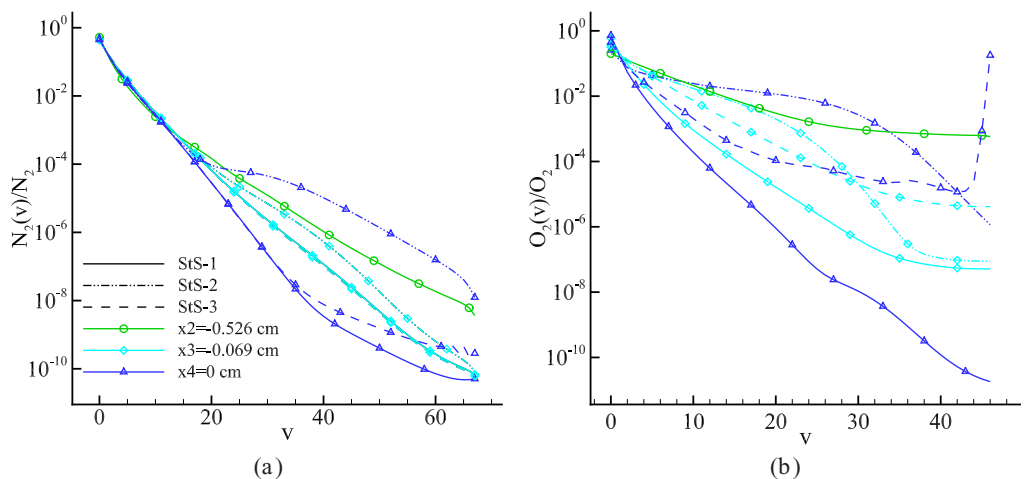


FIG. 10. Flow past a sphere: (a) N_2 and (b) O_2 vibrational distribution. Populations have been evaluated along the stagnation streamline and downstream of the shock wave at probes 2, 3, and 4, whose locations are given in Fig. 6(b).

catalysis of the wall and rarefaction effects, and they verify that, by tuning the recombination coefficients, they were able to match experimental findings. Differently from Cinquegrana *et al.* [30], in the present work a finite-rate partial catalytic model has been employed along with both a StS and a multitemperature model. With respect to the fully catalytic assumption, the finite-rate catalytic model provides results in better agreement with the experimental ones, demonstrating that in the considered hypersonic conditions a fully catalytic wall approximation cannot be assumed. Moreover, a closer gap between numerics and experiments has been found when the Park model is employed. On the other hand, when the StS is employed, better results have been found if recombination populates only the highest vibrational level. The multitemperature Park model was constructed adjusting Arrhenius rate parameters in order to reproduce experimental results, and therefore in some conditions it can better reproduce some experimental results, failing in different flow conditions. The discrepancies in the StS model are due to the uncertainties in the rate coefficients, which are calculated from basic principles. In this regard, it should be noted that quantifying the uncertainties in StS rates is not an easy task. While for N_2+N and O_2+O rates there is a good degree of confidence [48,49], molecule-molecule rates are poorly known. Approaches considering a forced harmonic oscillator [50,51], should be able to improve results, along with recent calculations by Valentini *et al.* [52] using the QCT approach on an *ab initio* potential energy surface. Another problem related to the StS model is the deactivation of vibrational levels on the surface whose rates are not known.

The use of different catalytic models put in evidence the role of the internal distribution of molecules desorbed by the surface. It is worth noting that the present chemical model neglects the contribution of ionization and electronically excited states that can explain the differences between experimental and theoretical heat fluxes, a subject that will be investigated in a future publication.

ACKNOWLEDGMENTS

This work was partially supported by the Italian Ministero dell'Istruzione, dell'Università e della Ricerca under the Programme Department of Excellence Legge 232/2016 (Grant No. CUP-D94I18000260001).

-
- [1] W. G. Vincenti and C. H. Kruger, *Introduction to Physical Gas Dynamics* (Wiley, New York, 1965), Vol. 246.
 - [2] C. Park, *Nonequilibrium Hypersonic Aerothermodynamics* (Wiley, New York, 1990).
 - [3] J. J. Bertin and R. M. Cummings, Fifty years of hypersonics: Where we've been, where we're going, *Prog. Aerosp. Sci.* **39**, 511 (2003).
 - [4] J. D. Schmisser, Hypersonics into the 21st century: A perspective on afosr-sponsored research in aerothermodynamics, *Prog. Aerosp. Sci.* **72**, 3 (2015).
 - [5] S. Tkatchova, Space debris mitigation, in *Emerging Space Markets* (Springer, Berlin, 2018), pp. 93–105.
 - [6] A. P. Kartashova, O. P. Popova, D. O. Glazachev, P. Jenniskens, V. V. Emel'yanenko, E. D. Podobnaya, and A. Y. Skripnik, Study of injuries from the chelyabinsk airburst event, *Planet. Space Sci.* **160**, 107 (2018).
 - [7] *Hypersonic Meteoroid Entry Physics*, edited by G. Colonna, M. Capitelli, and A. Laricchiuta, IOP Series in Plasma Physics (IOP, Bristol, 2019).
 - [8] P. N. Desai, D. T. Lyons, J. Tooley, and J. Kangas, Entry, descent, and landing operations analysis for the stardust entry capsule, *J. Spacecr. Rockets* **45**, 1262 (2008).
 - [9] S. Surzhikov, High-enthalpy radiating flows in aerophysics, in *Plasma Modeling: Methods and Applications*, Plasma Physics Series, edited by G. Colonna and A. D'Angola (IOP, Bristol, 2016), Chap. 12.
 - [10] M. Panesi, T. E. Magin, A. Bourdon, A. Bultel, and O. Chazot, Electronic excitation of atoms and molecules for the fire II flight experiment, *J. Thermophys. Heat Transf.* **25**, 361 (2011).

- [11] M. Auweter-Kurtz, H. L. Kurtz, and S. Laure, Plasma generators for re-entry simulation, *J. Propul. Power* **12**, 1053 (1996).
- [12] C. Purpura, F. De Filippis, P. Barrera, and D. Mandanici, Experimental characterisation of the cira plasma wind tunnel scirocco test section, *Acta Astronaut.* **62**, 410 (2008).
- [13] G. Colonna, M. Capitelli, M. Tuttafesta, and D. Giordano, Non-arrhenius no formation rate in one-dimensional nozzle airflow, *J. Thermophys. Heat Transf.* **13**, 372 (1999).
- [14] G. Colonna and M. Capitelli, Self-consistent model of chemical, vibrational, electron kinetics in nozzle expansion, *J. Thermophys. Heat Transf.* **15**, 308 (2001).
- [15] D. R. Olynick, W. D. Henline, L. H. Chambers, and G. V. Candler, Comparison of coupled radiative flow solutions with project fire II flight data, *J. Thermophys. Heat Transf.* **9**, 586 (1995).
- [16] F. Massobrio, R. Viotto, M. Serpico, A. Sansone, M. Caporicci, and J.-M. Muylaert, Expert: An atmospheric re-entry test-bed, *Acta Astronaut.* **60**, 974 (2007).
- [17] G. Colonna, F. Bonelli, and G. Pascazio, Impact of fundamental molecular kinetics on macroscopic properties of high-enthalpy flows: The case of hypersonic atmospheric entry, *Phys. Rev. Fluids* **4**, 033404 (2019b).
- [18] M. Capitelli, R. Celiberto, G. Colonna, F. Esposito, C. Gorse, K. Hassouni, A. Laricchiuta, and S. Longo, *Fundamental Aspects of Plasma Chemical Physics: Kinetics* (Springer Science & Business Media, New York, 2015), Vol. 85.
- [19] M. Capitelli, I. Armenise, D. Bruno, M. Cacciatore, R. Celiberto, G. Colonna, O. De Pascale, P. Diomede, F. Esposito, C. Gorse *et al.*, Non-equilibrium plasma kinetics: A state-to-state approach, *Plasma Sources Sci. Technol.* **16**, S30 (2007).
- [20] L. Cutrone, M. Tuttafesta, M. Capitelli, A. Schettino, G. Pascazio, and G. Colonna, 3d nozzle flow simulations including state-to-state kinetics calculation, *Proceedings of the XXIX International Symposium on Rarefied Gas Dynamics*, AIP Conf. Proc. No. 1628 (AIP, New York, 2014), p. 1154.
- [21] F. Esposito and M. Capitelli, Qct calculations for the process $N_2(v) + N \rightarrow N_2(v') + N$ in the whole vibrational range, *Chem. Phys. Lett.* **418**, 581 (2006).
- [22] R. Jaffe, D. Schwenke, G. Chaban, and W. Huo, Vibrational and rotational excitation and relaxation of nitrogen from accurate theoretical calculations, in *46th AIAA Aerospace Sciences Meeting and Exhibit* (AIAA, 2008), p. 1208.
- [23] J. D. Bender, P. Valentini, I. Nompelis, T. E. Schwartzentruber, and G. V. Candler, Characterization of vibrational and rotational energy transfer in N_2-N_2 dissociative collisions using the quasiclassical trajectory method, in *45th AIAA Thermophysics Conference* (AIAA, 2015), p. 3253.
- [24] R. S. Chaudhry, M. S. Grover, J. D. Bender, T. E. Schwartzentruber, and G. V. Candler, Quasiclassical trajectory analysis of oxygen dissociation via O_2 , O, and N_2 , in *2018 AIAA Aerospace Sciences Meeting* (AIAA, 2018), p. 0237.
- [25] D. Giordano, V. Bellucci, G. Colonna, M. Capitelli, I. Armenise, and C. Bruno, Vibrationally relaxing flow of n past an infinite cylinder, *J. Thermophys. Heat Transf.* **11**, 27 (1997).
- [26] F. Bonelli, M. Tuttafesta, G. Colonna, L. Cutrone, and G. Pascazio, An MPI-CUDA approach for hypersonic flows with detailed state-to-state air kinetics using a GPU cluster, *Comput. Phys. Commun.* **219**, 178 (2017).
- [27] M. Tuttafesta, G. Colonna, and G. Pascazio, Computing unsteady compressible flows using Roe's flux-difference splitting scheme on GPUs, *Comput. Phys. Commun.* **184**, 1497 (2013).
- [28] M. Tuttafesta, G. Pascazio, and G. Colonna, Multi-GPU unsteady 2D flow simulation coupled with a state-to-state chemical kinetics, *Comput. Phys. Commun.* **207**, 243 (2016).
- [29] S. Nonaka, H. Mizuno, K. Takayama, and C. Park, Measurement of shock standoff distance for sphere in ballistic range, *J. Thermophys. Heat Transf.* **14**, 225 (2000).
- [30] D. Cinquegrana, R. Votta, C. Purpura, and E. Trifoni, Continuum breakdown and surface catalysis effects in nasa arc jet testing at scirocco, *Aerosp. Sci. Technol.* **88**, 258 (2019).
- [31] G. Ranuzzi and S. Borreca, H3NS: code development verification and validation, Technical Report No. CIRA-CF-06-1017, CIRA (Italian Aerospace Research Centre, 2006).
- [32] G. A. Bird, The DS2V/3V Program Suite for DSMC Calculations, AIP Conf. Proc. No. 762 (AIP, New York, 2005), p. 541.

- [33] J. D. Anderson, *Hypersonic and High-Temperature Gas Dynamics, Second Edition* (AIAA Education Series, Reston, 2006).
- [34] I. Armenise, M. Barbato, M. Capitelli, and E. Kustova, State-to-state catalytic models, kinetics, and transport in hypersonic boundary layers, *J. Thermophys. Heat Transf.* **20**, 465 (2006).
- [35] G. Colonna, M. Capitelli, and D. Giordano, State to state electron and vibrational kinetics in supersonic nozzle air expansion: An improved model, in *Proceedings of the 33rd Plasmadynamics and Lasers Conference, Maui, Hawaii* (AIAA, Reston, VA, 2012), AIAA 2002-2163.
- [36] G. Colonna, M. Capitelli, L. D. Pietanza, A. Munafò, and M. Panesi, High-enthalpy ionized flows, in *Hypersonic Meteoroid Entry Physics*, IOP Series in Plasma Physics, edited by G. Colonna, M. Capitelli, and A. Laricchiuta (IOP, Bristol, 2019), Chap. 8.
- [37] A. Lemal, S. Nomura, and K. Fujita, Precursor ionization during high-speed earth entry, in *Hypersonic Meteoroid Entry Physics*, IOP Series in Plasma Physics, edited by G. Colonna, M. Capitelli, and A. Laricchiuta (IOP, Bristol, 2019), Chap. 9.
- [38] G. Colonna, L. D. Pietanza, and A. Laricchiuta, Ionization kinetic model for hydrogen-helium atmospheres in hypersonic shock tubes, *Int. J. Heat Mass Transf.* **156**, 119916 (2020).
- [39] R. N. Gupta, J. M. Yos, R. A. Thompson, and K.-P. Lee, *A Review of Reaction Rates and Thermodynamic and Transport Properties for an 11-Species Air Model for Chemical and Thermal Nonequilibrium Calculations to 30,000 K*, Ref. Publ. 1232 (NASA, 1990).
- [40] G. S. R. Sarma, Physico-chemical modeling in hypersonic flow simulation, *Prog. Aerosp. Sci.* **36**, 281 (2000).
- [41] R. B. Bird, W. E. Stewart, and E. N. Lightfoot, *Transport Phenomena*, 2nd ed. (Wiley, New York, 2002).
- [42] E. A. Mason and S. C. Saxena, Approximate formula for the thermal conductivity of gas mixtures, *Phys. Fluids* **1**, 361 (1958).
- [43] J. L. Steger and R. F. Warming, Flux vector splitting of the inviscid gas dynamic equations with application to finite-difference methods, *J. Comput. Phys.* **40**, 263 (1981).
- [44] F. Bonelli, M. Tuttafesta, G. Colonna, L. Cutrone, and G. Pascasio, Numerical investigation of high enthalpy flows, *Energy Proc.* **126**, 99 (2017).
- [45] M. Barbato, S. Reggiani, C. Bruno, and J. Muylaert, Model for heterogeneous catalysis on metal surfaces with applications to hypersonic flows, *J. Thermophys. Heat Transf.* **14**, 412 (2000).
- [46] M. Rutigliano, A. Pieretti, M. Cacciatore, N. Sanna, and V. Barone, N atoms recombination on a silica surface: A global theoretical approach, *Surf. Sci.* **600**, 4239 (2006).
- [47] L. Bedra, M. Rutigliano, M. Balat-Pichelin, and M. Cacciatore, Atomic oxygen recombination on quartz at high temperature: Experiments and molecular dynamics simulation, *Langmuir* **22**, 7208 (2006).
- [48] F. Esposito, I. Armenise, and M. Capitelli, N-N₂ state to state vibrational-relaxation and dissociation rates based on quasiclassical calculations, *Chem. Phys.* **331**, 1 (2006).
- [49] F. Esposito, I. Armenise, G. Capitta, and M. Capitelli, O-O₂ state to state vibrational-relaxation and dissociation rates based on quasiclassical calculations, *Chem. Phys.* **351**, 91 (2008).
- [50] M. L. da Silva, V. Guerra, and J. Loureiro, A review of non-equilibrium dissociation rates and models for atmospheric entry studies, *Plasma Sources Sci. Technol.* **18**, 034023 (2009).
- [51] M. Lino da Silva, J. Loureiro, and V. Guerra, A multiquantum dataset for vibrational excitation and dissociation in high-temperature O₂-O₂ collisions, *Chem. Phys. Lett.* **531**, 28 (2012).
- [52] P. Valentini, T. E. Schwartzentruber, J. D. Bender, I. Nompelis, and G. V. Candler, Direct molecular simulation of nitrogen dissociation based on an ab initio potential energy surface, *Phys. Fluids* **27**, 086102 (2015).